Bioorganic & Medicinal Chemistry Letters 20 (2010) 7132–7136

Contents lists available at ScienceDirect

Bioorganic & Medicinal Chemistry Letters

journal homepage: www.elsevier.com/locate/bmcl

Synthesis and structure–activity relationships of tyrosine-based inhibitors of autotaxin (ATX)

James E. East [a,*], Andrew J. Kennedy [a], Jose L. Tomsig [b], Alexandra R. De Leon [b], Kevin R. Lynch [b], Timothy L. Macdonald [a,b,*]

[a] University of Virginia, Department of Chemistry, PO Box 400319, McCormick Road, Charlottesville, VA 22904, United States
[b] University of Virginia, Department of Pharmacology, 1340 Jefferson Park Avenue, Charlottesville, VA 22908, United States

ARTICLE INFO

Article history:
Received 2 August 2010
Revised 3 September 2010
Accepted 7 September 2010
Available online 15 September 2010

Keywords:
Lysophosphatidic acid
Autotaxin
Structure–activity relationships
Hansch linear free energy relationship

ABSTRACT

Autotaxin (ATX) is a secreted soluble enzyme that generates lysophosphatidic acid (LPA) through its lysophospholipase D activity. Because of LPA's role in neoplastic diseases, ATX is an attractive therapeutic target due to its involvement in LPA biosynthesis. Here we describe the SAR of ATX inhibitor, VPC8a202, and apply this SAR knowledge towards developing a high potency inhibitor. We found that electron density in the pyridine region greatly influences activity of our inhibitors at ATX.

Autotaxin (ATX) is an enzyme in the nucleotide phosphatase/pyrophosphatase 2 (NPP2) family of enzymes and it is the only NPP2 with lysophospholipase D activity. ATX catalyzes the hydrolysis of lysophosphatidylcholine (LPC) to yield lysophosphatidic acid (LPA) which signals cells via a set of five G-protein coupled receptors (GPCRs). Originally identified as an autocrine growth factor,[1] ATX is implicated in tumor progression because of LPA's role in cell migration and invasiveness.[2] As a result there has been considerable interest in targeting ATX with small molecules to affect LPA driven neoplastic diseases.[3,4]

LPA has been demonstrated to be a feedback inhibitor of ATX.[5] With this in mind our laboratories have set out to develop LPA analogs as ATX inhibitors (Fig. 1). Our earliest series of LPA analogs were made as probes of the various receptors. These molecules featured the *N*-acyl ethanolamide phosphoric acid (NAEPA) backbone, which was a modification of the natural glycerol moiety in LPA.[6] The NAEPA compounds eventually evolved into LPA analogs containing various amino acids other than glycine[7] with L-tyrosine analogs exhibiting the most useful activities.[8] Phosphate head group mimetics including phosphonic and thiophosphonic acid derivatives[9] and substituted phosphonates[10,11] were also investigated because of enhanced metabolic stability.

From these compounds, **5a(anti)** (VPC8a202) (Fig. 1) was found to be a potent inhibitor (K_i = 1 μM) of ATX. However, a clear

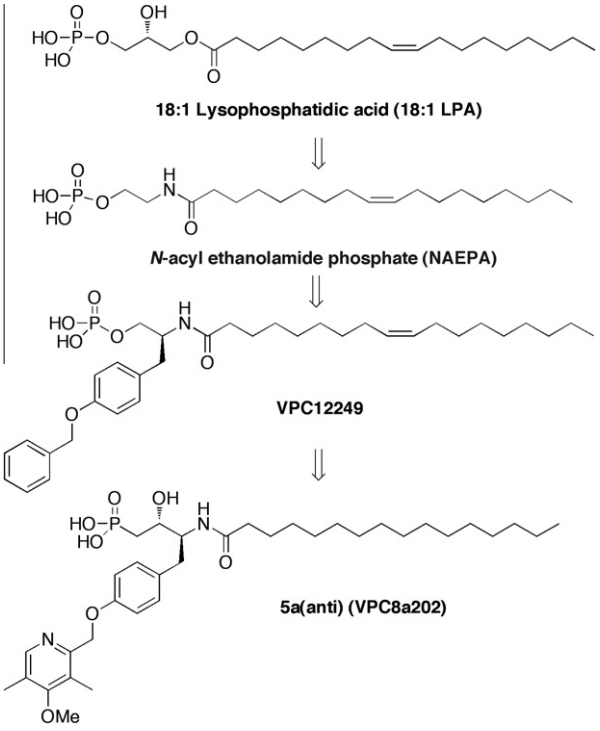

Figure 1. Evolution of tyrosine-based LPA analog **5a(anti)** (VPC8a202).

* Corresponding authors. Tel.: +1 434 924 7718 (J.E.).
E-mail addresses: je5y@virginia.edu (J.E. East), tlm@virginia.edu (T.L. Macdonald).

0960-894X/$ - see front matter © 2010 Elsevier Ltd. All rights reserved.
doi:10.1016/j.bmcl.2010.09.030

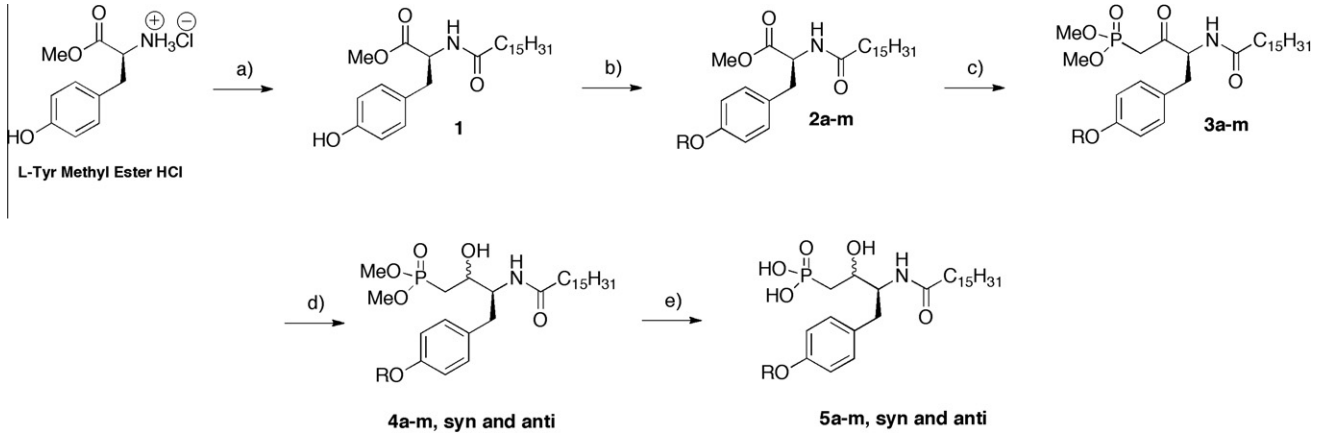

Scheme 1. Reagents and conditions: (a) palmitoyl Cl, DIEA, DCM, 0 °C; (b) ROMs (or RBr), K_2CO_3, 18-crown-6, acetone, 70 °C; (c) dimethyl methylphosphonate, *n*BuLi, −78 °C; (d) $CeCl_3{\cdot}7H_2O$, $NaBH_4$, EtOH:THF, 0 °C; (e) TMSBr, DCM 0 °C to rt.

structure–activity relationship of the pyridyl region remained unexplored and this information is needed for our future efforts towards more potent inhibitors of ATX. Therefore, we report herein the synthesis and SAR studies of a series of tyrosine-based analogs of **5a(anti)** (VPC8a202).

Synthesis of the β-hydroxy phosphonates (Scheme 1) began with acid chloride coupling of palmitoyl chloride with L-tyrosine methyl ester hydrochloride to give amide **1**. Benzylic meslates or bromides were coupled to the phenol of **1** in the presence of potassium carbonate and 18-crown-6 in refluxing acetone to give compounds **2a**–**m**. Next, treatment of intermediates **2a**–**m** with dimethyl methylphosphonate and *n*-butyllithium in THF at −78 °C afforded β-keto phosphonates **3a**–**m**. Reduction of the ketone under Luche conditions[12] yielded protected β-hydroxy phosphonates **4a**–**m**. The resulting diastereomers were separated by flash chromatography. Designations of **syn** and **anti** were arrived at through the use of stereochemical studies performed by Peng et al.[11] and homology modeling studies using ATX with our compounds (vide infra). Finally, bromotrimethylsilane (TMSBr) treatment with subsequent silyl cleavage in MeOH:H_2O afforded the deprotected phosphonates **5a**–**m**, diastereomers **syn** and **anti**.

All compounds were tested for their inhibitory capability in a serum based in vitro assay (see Supplementary data). The deletion of the nitrogen heteroatom (Table 1) and methyl substituents (**5b(anti)**/**(syn)**) from **5a(anti)** showed a significant loss in activity. Retention of the nitrogen heteroatom (**5c(anti)**), plus methoxy substituents (**5d(anti)**/**5d(syn)**) or alkyl groups (**5e(anti)**) allowed for near equipotent compounds in relation to **5a(anti)**. Elongation of the methoxy groups to ethoxy (**5f(anti)**/**(syn)**) and propoxy (**5g(anti)**/**(syn)**) led to a progressive loss in activity. **5i(anti)**/**(syn)**, **5m(anti)**, and **5k(anti)**/**(syn)** retained potency while containing no nitrogen heteroatom yet retaining methoxy and/or methyl groups. Interestingly, the dichlorinated aryl ethers, **5j(anti)**/**(syn)**, proved to be the least potent in this series of compounds. This result is presumably from the electron withdrawing capability of the chlorines.

A molecular docking analysis was performed with the utilization of a previously reported homology model of the catalytic domain of ATX by Parrill et al.[13] which was derived from the solved Xac NPP crystal stucture (entry 2GSU[14] in the Protein Data Base). Docking studies with **5a(anti)** showed a series of low energy possible binding conformations; all of which presented the phosphonate within 5 Å of Thr210 and the two zinc metal centers of the active site (Fig. 2). These studies also revealed that the saturated tail of **5a(anti)** fills the large lipophilic pocket also found to bind the lipid tail of LPC. The anti configuration of the beta alcohol

Table 1
In vitro activities for compounds **5a**–**m**

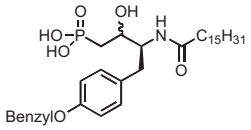

Compound	Benzyl group	K_i (μM)
5a(anti)	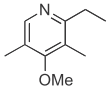	1.0
5a(syn)		3.9
5b(anti)		27.0
5b(syn)		83.0
5c(anti)		4.4
5c(syn)		11.0
5d(anti)		1.5
5d(syn)		3.5
5e(anti)	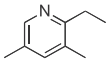	3.9
5e(syn)		399.0
5f(anti)	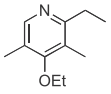	4.7
5f(syn)		6.2
5g(anti)	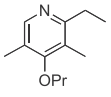	8.8
5g(syn)		11.1
5h(anti)		11.6
5h(syn)		22.5
5i(anti)	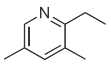	1.8
5i(syn)		4.8
5j(anti)	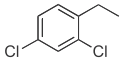	584.1
5j(syn)		1059.2
5k(anti)	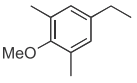	1.6
5k(syn)		5.3
5l(anti)	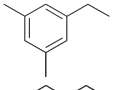	88.9
5l(syn)		217.5
5m(anti)	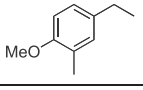	4.3
5m(syn)		26.5

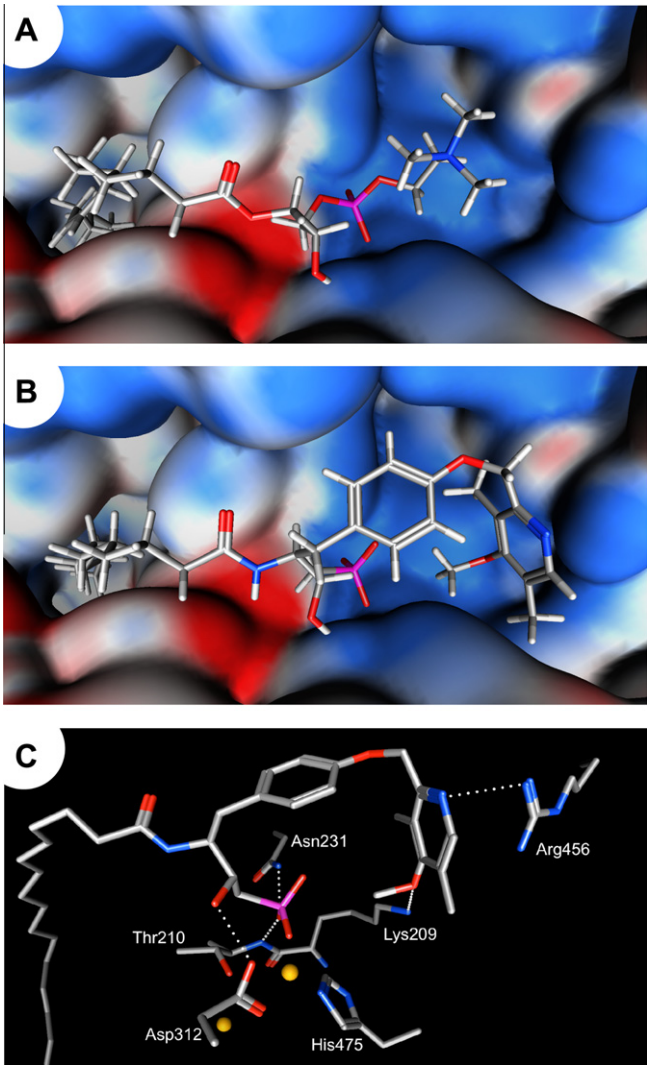

Figure 2. ATX homology model with LPC 18:1 and **5a(anti)**. (A) ATX shown as an electrostatic surface (uncharged = white, positive = blue, and negative = red) with LPC 18:1 shown as a stick model. (B) ATX shown as an electrostatic surface with **5a(anti)** shown as a stick model. (C) Close up of ATX active site with important residues and **5a(anti)** shown as stick models. Hydrogen bonds and arene–cation interactions shown as dotted white lines. Zinc cations shown as yellow spheres.

present in **5a(anti)** forms a weak hydrogen bond with the zinc co-ordinating Asp312 residue,[14] that may explain the stereo preference for the anti beta alcohol over the syn relationship. One interesting development was the evidence that the substituted pyridine of **5a(anti)** binds the hydrophilic leaving group pocket of ATX, and the tyrosine core acts almost solely as a linker to facilitate this interaction. Specifically, the model suggests an aromatic–guanidine interaction with Arg456 and a weak hydrogen bond between the methoxy substituent at the 4-position and Lys209 (Fig. 2C). Docking analysis of the full library of aryl derivatives (**5a**–**m**) showed similar results, with the degree of interaction depending on aryl ring electron density and geometric fit in the pocket.

For each member of the aryl derivative library (**5a**–**m**), three docking scores (London dG, Affinity dG, and Alpha HB) available in MOE[15] were used to judge different binding conformation possibilities. The long acyl chains (C15) were considered only for the lead **5a** and was not varied for the other library members. Even though there were a number of similarly scored conformations for the acyl chain of **5a(anti)**, they led to negligible differences in the orientation of the tyrosine linker, phosphinated and pyridyl group. One conformation of the acyl chain was then conserved for every member of the library not for its accuracy, but to limit the test set for docking analysis. In most cases, a single conformation scored best in two or three of the possible conformers, and in fact all three scoring functions proved capable of producing similar lowest energy binding conformations. However, in analyzing the library as a whole, Alpha HB was the only scoring function to correlate with statistical relevance to activity (Fig. 3A). All library members preferably docked in a conformation similar to that of **5a(anti)**, where the tyrosine core acts as a linker to display the benzyl group of the inhibitor to the leaving group pocket of ATX. Alpha HB, a scoring function based on geometrical fit, was able to accurately explain activity by how well the substituents filled the pocket, as well as how closely the benzyl group interacted with Arg456. Substituents that add electron density into the π system of the benzyl group had closer association with Arg456 (**5a(anti)** = 2.2 Å, **5j(anti)** = 3.9 Å), and therefore scored better. There is also a steric effect with substitution that if exceeded lead to dissociation of the benzyl group from the pocket, explaining the linear decrease in activity from **5a** to **5f** to **5g**.

The homology model docking study predicts the interaction between the aromatic π systems of **5**(**a**–**m**) and the guanidine of Arg456 to be a principle component in binding affinity of the aryl system. Therefore, there should be a negative relationship between Hammett substituent constants (σ) and pK_i, since the arene–cation bond is dependant on aryl electron density. The system was evaluated using a Hansch linear free energy model,[16] and the aromatic derivatives were divided into individual substituents and each

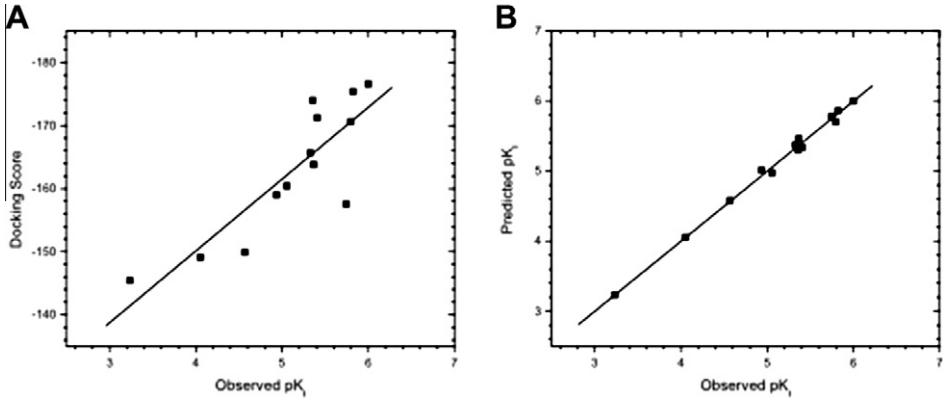

Figure 3. Docking and Hansch model studies. (A) Experimental pK_i—docking score plot (R^2 = 0.72833) calculated with MOE Alpha HB scoring function for minimized docking conformations (see Supplementary data for details). (B) Hansch linear free energy linear model (R^2 = 0.99416) based on the electronic, steric and solubility effects of aryl substitution described in Table 2.

Table 2
Hansch linear free energy model data set

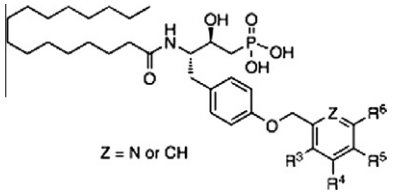

Compound	pK_i	Prod. pK_i[d]	*z*-Score	Aromatic substitution				Hammell value (op)[a]				van der Walls volume (Å)[b]				*n*[c]
				3	4	5	6	3	4	5	6	3	4	5	6	
5a	6.00	6.00	0.00	Me	OMe	Me	H	−0.17	−0.27	−0.17	0	31.5	37.1	31.5	10.4	−0.90
5b	4.55	4.58	0.38	H	H	H	H	0	0	0	0	10.4	10.4	10.4	10.4	0.00
5c	5.36	5.63	1.01	H	H	H	H	0	0	0	0	1.04	10.4	10.4	10.4	−1.27
5d	5.82	5.86	0.63	H	OMe	H	H	0	−0.27	0	0	10.4	37.1	10.4	10.4	1.45
5e	5.41	5.34	1.19	Me	H	Me	H	−0.17	0	−0.17	0	31.5	10.4	31.5	10.4	−0.30
5f	5.33	5.37	0.74	Me	OEt	Me	H	−0.17	−0.24	−0.17	0	31.5	55.9	31.5	10.4	−0.56
5g	5.06	4.97	1.40	Me	OPt	Me	H	−0.17	−0.25	−0.17	0	31.5	73.5	31.5	10.4	0.06
5h	4.94	5.01	1.35	Me	OCH_2CF_3	Me	H	−0.17	−0.21	−0.17	0	31.5	64.8	31.5	10.4	−0.13
5i	5.74	5.77	0.51	Me	H	Me	H	−0.17	0	−0.17	0	31.5	10.4	31.5	10.4	0.97
5j	3.23	3.23	0.00	Cl	H	Cl	H	0.23	0	0.23	0	28.5	10.4	28.5	10.4	1.05
5k	5.80	5.76	1.65	H	Me	OMe	Me	0	−0.17	−0.27	−0.17	10.4	31.5	37.12	31.5	0.45
5l	4.05	4.05	0.00	H	Me	H	Me	0	−0.17	0	−0.17	10.4	31.5	10.4	31.5	1.05
5m	5.37	5.46	1.65	H	H	OMe	Me	0	0	−0.27	−0.17	10.4	10.4	37.13	31.5	0.12
Relative importance of descriptions								0.60	0.53	0.70	0.00	1.00	0.57	0.70	0.79	0.51

[a] Ref. 17.
[b] Ref. 18.
[c] $z_a = C\,\mathrm{Lop}\,P_i - C\,\mathrm{Log}\,P$ **5b**.
[d] Prod. pK_i = (−3.34 (3op) − 2.94 (4op) − 3.36 (5op)) + (−0.0627 (3 vol) − 0.0170 (4 vol) + 0.0438 (5 vol) − 0.0579 (6 vol)) + 0.0261 (x) − 0.467 ($-x^2$) + 5.55.

substituent described by its Hammett value,[17] van der Waals volume,[18] and difference in *C* log *P* (π) from the unsubstituted benzyl derivative **5b** (Table 2). This Hansch linear free energy model (Fig. 3B) showcases the relationship the electron density of the aromatic region of this class of inhibitors, when corrected for steric effects and *C* log *P*. There is a negative relationship between Hammet value and pK_i at the 3, 4, and 5 positions of the benzyl ring, which shows the preference for electron rich aromatics and supports the results from the docking study (Table 2). The Hansch analysis also corrects for substituent steric effects, which were compared using the van der Waals volumes, and indicated the substitution was least tolerated at the 3-position and most tolerated at the 5-position of the ring.

In summary, we set out to determine what elements were important in the pyridine ring of the ATX inhibitor **5a(anti)** (VPC8a202). Our compounds are comparable to other reported potent ATX inhibitors that were tested in our choline release assay. These tyrosine derivatives share the common features of HA51, HA130,[19] S32826,[20] and Br-LPA[21] (Table 3) in that they have an electrophilic head group and a hydrophobic tail region. Through the use of classical SAR and QSAR we discovered that potency of our compound library increased with increasing electron density contained in the pyridine ring. Our use of homology modeling suggests that this trend may be due to an interaction with the pyridine group and Arg456. We hope to use these findings to aid us in our work towards further validating the homology model and, ultimately, developing more potent inhibitors of autotaxin.

Table 3
Reported ATX inhibitors tested in choline release assay

Name	Structure	K_i (μM)
HA130	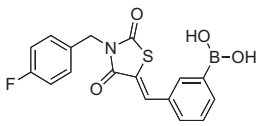	0.094
HA51	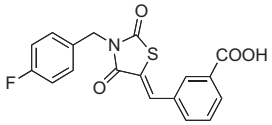	0.187
S32826	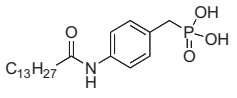	0.367
Br-LPA	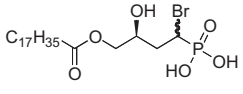	40.1

Acknowledgment

This work is supported by NIH grants R01 GM052722, R01 GM067958.

Supplementary data

Supplementary data associated with this article can be found, in the online version, at doi:10.1016/j.bmcl.2010.09.030.

References and notes

1. Stracke, M. H.; Krutzsch, H. C.; Unsworth, E. J.; Arestad, A.; Cioce, V.; Schiffmann, E. *J. Biol. Chem.* **1992**, *267*, 2524.
2. Mills, G. B.; Moolenaar, W. H. *Nat. Rev. Cancer* **2003**, *3*, 582.
3. Albers, H.; van Meeteren, L.; Egan, D.; van Tilburg, E.; Moolenaar, W.; Ovaa, H. *J. Med. Chem.* **2010**, *13*, 4958.
4. North, E.; Howard, A.; Wanjala, I.; Pham, T.; Baker, D.; Parrill, A. *J. Med. Chem.* **2010**, *53*, 3095.
5. Meeteren, L.; Ruurs, P.; Christodoulou, E.; Goding, J.; Takakusa, H.; Kikuchi, K.; Perrakia, A.; Nagano, T.; Moolenaar, W. *J. Biol. Chem.* **2005**, *280*, 21155.
6. Hook, S.; Ragan, S.; Hopper, D.; Honemann, C.; Durieux, M.; Macdonald, T.; Lynch, K. *Mol. Pharm.* **1998**, *53*, 188.
7. Heasley, B.; Jarosz, R.; Lynch, K.; Macdonald, T. *Bioorg. Med. Chem. Lett.* **2004**, *14*, 2735.

8. Heasley, B.; Jarosz, R.; Carter, K.; Van, S.; Lynch, K.; Macdonald, T. *Bioorg. Med. Chem. Lett.* **2004**, *14*, 4069.
9. Santos, W.; Heasley, B.; Jarosz, R.; Lynch, K.; Macdonald, T. *Bioorg. Med. Chem. Lett.* **2004**, *14*, 3473.
10. Cui, P.; Tomsig, J.; McCalmont, W.; Lee, S.; Becker, C.; Lynch, K.; Macdonald, T. *Bioorg. Med. Chem. Lett.* **2007**, *17*, 1634.
11. Cui, P.; McCalmont, W.; Tomsig, J.; Lynch, K.; Macdonald, T. *Bioorg. Med. Chem.* **2008**, *16*, 2212.
12. Luche, J. L. *J. Am. Chem. Soc.* **1978**, *100*, 2226.
13. Parrill, A. L.; Echols, U.; Nguyen, T.; Pham, T.-C. T.; Hoeglund, A.; Baker, D. L. *Bioorg. Med. Chem.* **2008**, *16*, 1784.
14. Zalatan, J. G.; Fenn, T. D.; Brunger, A. T.; Herschlag, D. *Biochemistry* **2006**, *45*, 9788.
15. Molecular Operating Environment (MOE 2009.10); C.C.G., Inc., 1010 Sherbrooke West, Suite 910, Montreal, Quebec, Canada H3A 2R7.
16. (a) Hansch, C.; Muir, R. M.; Fujita, T.; Miloney, P. P.; Geiger, F.; Streich, M. *J. Am. Chem. Soc.* **1963**, *85*, 2817; (b) Hansch, C.; Fukunaga, J. Y.; Jow, Y. C. *J. Med. Chem.* **1977**, *20*, 96.
17. (a) Hammett, L. P. *J. Am. Chem. Soc.* **1937**, *59*, 96; (b) Charton, M. *J. Org. Chem.* **1963**, *28*, 3121.
18. Ertl, P.; Rohde, B.; Selzer, P. *J. Med. Chem.* **2000**, *43*, 3714.
19. Albers, H.; Dong, A.; van Meeteren, L. A.; Egan, D.; Sunkara, M.; van Tilburg, D.; Schuurman, K.; van Tellingen, O.; Morris, A.; Smyth, S.; Moolenaar, W.; Ovaa, H. *Proc. Natl. Acad. Sci. U.S.A.* **2010**, *107*(16), 7257.
20. Ferry, G.; Moulharat, N.; Pradere, J.; Desos, P.; Try, A.; Genton, A.; Giganti, A.; Beucher-Gaudin, M.; Lonchampt, M.; Bertrand, M.; Saulnier-Blache, J.; Tucker, G.; Cordi, A.; Boutin, J. *J. Pharmacol. Exp. Ther.* **2008**, *327*, 809.
21. Zhang, H.; Xu, X.; Gajewiak, J.; Tsukahara, R.; Fujiwara, Y.; Liu, J.; Fells, J.; Perygin, D.; Parrill, A.; Tigyi, G.; Prestwich, G. *Cancer Res.* **2009**, *69*, 5441.